A modified log-law of flow velocity distribution in partly obstructed open channels

Environ Fluid Mech
DOI 10.1007/s10652-015-9439-7

ORIGINAL ARTICLE

A modified log-law of flow velocity distribution in partly obstructed open channels

Mouldi Ben Meftah[1] · **Michele Mossa**[1]

Received: 14 January 2015 / Accepted: 7 December 2015

Abstract Flow through rigid and emergent/submerged cylinder arrays are commonly found in several engineering application such as offshore structures, transmission lines, chimneys, array of silos and field array of trees. Various hydrodynamic phenomena may be occurring in the interaction between a flowing fluid and these structures. In this manuscript we focus on the study of flow structures in a channel partially obstructed by an array of equi-spaced, vertical, rigid, emergent, circular steel cylinders. Experimental results show that the presence of the cylinders array strongly affects the flow velocity distribution, forming a transversal sharp transition region at the interface between the obstructed and the unobstructed domains. At the interface, for the current and previous studies, it was observed that the flow distribution always resembles a boundary layer feature. This similarity in feature of the flow distribution as a boundary layer has led to adapting the universal law of the wall to describe the transversal profile of the mean flow velocity, considering, by analogy, the interface separating both domains as a virtual wall. The specific objectives addressed in this study is to propose and validate a new modified log-law predicting the representative transversal profile of the mean flow velocity at the interface between the obstructed and the unobstructed domains. The proposed analytical model is validated by a series of experiments carried out on a very large rectangular channel in the Department of Civil, Environmental, Building Engineering and Chemistry of the Technical University of Bari—Italy. The three-dimensional flow velocity components were measured using a 3D Acoustic Doppler Velocimeter ADV. As a result, it is observed that the measured and the predicted, applying the proposed modified log-law, mean flow velocity data have a perfect matching between them. Moreover, in the second

✉ Mouldi Ben Meftah
mouldi.benmeftah@poliba.it

Michele Mossa
michele.mossa@poliba.it

[1] Department of Civil, Environmental, Building Engineering and Chemistry, Technical University of Bari, Via E. Orabona 4, 70125 Bari, Italy

Published online: 21 December 2015

part of the paper, detailed observations on the flow turbulence structure are analyzed and discussed.

Keywords Partly obstructed open channels · Emergent cylinder arrays · Shear layer · Velocity distribution · Transversal profiles · Law of the wall · Turbulence structure

Notations

A, B	Empirical constants (−)
a	Total frontal area (area exposed to the flow) per unit array (m^{-1})
B_c	Channel width (m)
b	Width of the unobstructed area (m)
C_D	Drag coefficient (−)
d	Cylinder diameter (m)
Fr_0	Inlet Froude number (−)
Fr_2	Froude number in the unobstructed area (−)
g	Gravity acceleration ($m.s^{-2}$)
H	Flow depth (m)
h	Cylinder height (m)
I	Energy slope (−)
k_s	Representative of roughness height (m)
k_s^+	Dimensionless roughness height (−)
L	Secondary velocity intensity coefficient (−)
N	Time series length of velocity sampling
n	Density of cylinders (stem m^{-2})
Q	Channel discharge ($m^3\ s^{-1}$)
Re_0	Inlet Reynolds number (−)
Re_2	Reynolds number in the unobstructed area (−)
s, s_x, s_y	Space between cylinders (m)
T	Water temperature (°C)
t	Time (s)
U,V	Streamwise and spanwise time-averaged velocity (ms^{-1})
U_m, V_m	Streamwise and spanwise velocity at the effective shear layer origin (ms^{-1})
U_N	Mean velocity of N samplings
U_0	Mean channel velocity upstream of the cylinder arrays (ms^{-1})
U_1	Flow velocity inside the obstructed region (ms^{-1})
U_2	Flow maximum velocity in the unobstructed area (ms^{-1})
U^+, U^{++}	Dimensionless streamwise velocities (−)
$u*$	Friction velocity (ms^{-1})
u', v'	Longitudinal and transversal velocity fluctuations (ms^{-1})
x, y, z	Longitudinal, transversal and vertical coordinates, respectively (m)
x_{eq}	Equilibrium velocity length (m)
Y	Width of the obstructed area (m)
y_m	Effective shear layer origin (m)
y^+, y^{++}	Dimensionless transversal coordinates (−)
α_1, α_2	Empirical constants (−)
β_1	Dimensionless velocity parameter (−)
β_2	Dimensionless length parameter (−)
δ_1	Inner layer width (m)

δ_2	Outer layer width (m)
Φ, Φ'	Integration constant (−)
φ	volume solid fraction of the cylinders (−)
κ	Von Karman's constant (−)
ν	Fluid kinematic viscosity ($m^2\ s^{-1}$)
ν_t	Eddy viscosity ($m^2\ s^{-1}$)
θ	Momentum thickness (m)
θ_{eq}	Momentum thickness at the equilibrium stage (m)

1 Introduction

Natural channels are commonly characterized by a main channel for primary flow conveyance and an overbank, or floodplain, with diminished conveyance capacity and/or flood storage area. Previous efforts to estimate the flow resistance in compound channels have focused on the boundary shear and the gravitational forces that exist at the main channel-floodplain interface. However, the flow resistance at the interface is also a function of the turbulence intensities or momentum transfer [1]. At the interface between the array of cylinders/vegetation and the unobstructed flow areas, the transfer of momentum takes the form of an apparent shear stress [2–4]. An estimation only of the flow resistance based on an overall force balance concept is not able to explain all the flow hydrodynamic characteristics in the interface region. In fact, the aquatic vegetation in a natural environment is characterized by multiple aspects, i.e. it can be submerged or emerged, rigid or flexible, leafed or leafless, have branches or rods, with high or low density, along the entire width or a portion of the stream. It is also difficult to measure and interpret all the vegetation properties referring to data collected from real channels with live vegetation [5–7]. Thence and despite the many studies conducted on partly obstructed channel flows, this issue remains of fundamental importance where there is so much to understand, to discover and to be done.

White and Nepf [4] carried out detailed 2D flow velocity measurements with a Laser Doppler Velocimeter (LDV) in a 1.2 m wide, 13 m long flume, partially obstructed with a 0.4 m wide array of wooden, emergent, circular cylinders of three different volume densities ($\varphi = 0.02$, 0.045 and 0.10). The authors observed that at the interface between the obstructed and the unobstructed domains a shear layer is found, possessing two distinct length scales: (i) an inner-layer thickness set by the array resistance (ii) a wider outer region, which resembles a boundary layer, has a width set by the water depth and bottom friction. The authors argued that the interfacial Reynolds shear stress approximately balances the array resistance in the sharp transition region across the interface. While, in the boundary layer outside the array, the shear stress approximately balances the pressure gradient from the free-surface slope. According to the authors, as the flow develops, the peak of the Reynolds stress shifts toward the interface and becomes more pronounced. Moreover, they observed that this peak in the equilibrium Reynolds stress profile coincides with the velocity inflection point, which is within 1–2 cm of the array edge and it is a point of high energy production.

White and Nepf [4] assumed that the shear layer is unaffected by the cylinders array, which is not always valid. The free shear layer, formed at the interface, is subjected to transversal motion and may be shifted (increase of its width) away from the geometrical

edge of the obstructed area [2, 8]. The longitudinal vorticity source, which is attenuated within the obstructed domain, increases externally leading to an overall increase of the effects of the secondary velocities [2]. In the unobstructed flow region, flow features resemble those of the boundary layer, whereas in the obstructed region the flow has the features of "porous obstructions" [8–11]. In a rectangular open channel with vegetated bank, Naot et al. [2], analyzing the streamwise velocity distribution through the channel cross-section, observed that the flow velocity at the interface is affected by the vegetation density. For a volume density $\varphi < 0.03$, they indicated that the vegetation affects the flow like a rough bank introducing asymmetry in the unobstructed channel area (density values in Ben Meftah et al.s [8] are included in this range). For $0.03 < \varphi < 0.13$, however, the flow in the obstructed area is gradually blocked (minimum effect on the free shear layer), making the flow pattern in the unobstructed area similar to that of a wide symmetric channel (density values in White and Nepf's [4] are included in this range). For $\varphi > 0.13$, an asymmetry, due the intensive secondary currents, of the flow velocity in the unobstructed area and a shift of the velocity maximum away from the interface were experienced. Moreover, the authors concluded that the location of the free shear layer varies from case to case.

Many experimental and numerical studies [3, 4, 12, 13] have indicated the formation of coherent vortex structures at the interface between the obstructed and unobstructed areas. Due to the drag discontinuity at this interface, the velocity profile in the shear layer exhibits an inflection point that is unstable and promotes the growth of Kelvin–Helmholtz vortices [14]. Moving further downstream, the vortices grow in size to reach a fully-developed stage, from where the transversal profiles of the flow velocity remains almost invariant varying the downstream position.

Rominger and Nepf [14] indicated that, upstream of an obstructed area of a finite-width, the flow adjusts over an interior length scale proportional to the drag length scale and the width Y (full width of the obstructed area perpendicular to the oncoming flow) of the obstructed area,. This length scale depends on a non-dimensional flow-blockage parameter of the obstructed domain, described by $C_D a(Y/2)$, where C_D is the drag coefficient within the array of cylinders, on which several studies have been conducted to estimate it [15–20], $a = nd$ is the total frontal area (area exposed to the flow) per unit array, d is the cylinder diameter and n is the density of cylinders per unit surface. For low flow-blockage canopies $[C_D a(Y/2) << 1]$, the interior adjustment length is set by the obstructed drag scale $(C_D a)^{-1}$. For high flow-blockage canopies $[C_D a(Y/2) >> 1]$, the adjustment length is set by the half-width, $Y/2$. The transition between the two regimes is expected to occur when $Y/2 \approx (C_D a)^{-1}$. Downstream of the interior adjustment region, the authors indicated the formation of a shear layer along the flow-parallel to the interface between the array and the unobstructed flow.

There are many examples of flow encountering fixed porous obstructions. In literature [14] such obstructions are referred to as canopies. As an example, planting of random or regular arrays of trees can be used as a protection and management system of floodplains and banks. Agriculture canopies are porous obstructions, where fields of trees can be organized in regular square rows. In addition, flow through rigid and emergent cylinder arrays are commonly found in several engineering application such as offshore structures, transmission lines, chimneys and array of silos. Several of these structures may also show geometries similar to the model geometry investigated in this manuscript. In the present study, we focus on the understanding of the various hydrodynamic phenomena occurring in the interaction between a flowing fluid and these structures.

Several methods exist to predict vertical velocity distribution and to estimate bed shear stress in rough channels without vegetation, the best known methods is still the logarithmic law of the wall. The presence of vegetation in the aquatic environment considerably alters the turbulent flow structures. The additional drag exerted by this vegetation largely influences the distribution of mean and instantaneous velocity. Numerous experimental studies conducted on submerged vegetated channels have shown that the vertical velocity profile above aquatic vegetation follows a logarithmic trend. Therefore, many of these studies adapted the universal logarithmic law of the wall, with specific modifications, to describe this velocity profile. Different methods adapting the vertical velocity profile over aquatic vegetation to the Prandtl's log-law are well summarized in a previous study by Stephan and Gutknecht [21]. At the interface between the obstructed and the unobstructed flow areas of the present study and other previous studies [4, 8, 12, 22], independent of the obstructed area characteristics, it was observed that the transversal streamwise velocity distribution almost behaves the same way as a vertical velocity profile above aquatic vegetation, following a logarithmic trend. This similarity between both cases also made us adapting the universal logarithmic law of the wall, to describe the transversal mean velocity profile at the interface in a partly vegetated channel.

Despite the numerous previous studies on partly obstructed channels by array of rigid and emergent cylinders/vegetation, it was remarked a lack of methods adapting the universal logarithmic law to the transversal velocity profile at the interface. This motivated us to enhance this topic by adapting the log-law to predict the transversal profile of the flow mean velocity at the interface.

This study proposes a new modified log-law adapting the transversal profile of the flow mean velocity at the interface between the obstructed and unobstructed areas in a partially obstructed channel by an array of emergent cylinders/vegetation. As a part of second interest, detailed observations on the flow turbulence structure are also analyzed and discussed.

2 Theoretical approach

Along the transversal direction, the turbulent flow in partially obstructed rectangular channels can be divided into two sub-regions, the obstructed region and the unobstructed region. In the case where the mean flow depth, H, is much smaller than the mean channel width, B_c, that is $H/B_c << 1$, the flow can be considered, approximately, bi-dimensional (x, y), in which x and y are the longitudinal and transversal directions, respectively (Fig. 1). In the present study, the obstructed region was simulated by an array of vertical steel cylinders. Cylinders were arranged regularly and spaced longitudinally, s_x, and transversally, s_y, with the same distance $s = s_x = s_y$ (see Fig. 1). The volume solid fraction of the cylinders is defined as: $\varphi = \pi ad/4$.

The velocity inside the obstructed region (defined as a time and spatially average pore velocity) was defined as U_1. Through the shear layer region across the interface, the flow velocity gradually increases to reach a maximum and constant velocity U_2 in the main channel. The velocity distribution is characterized by two length scales: δ_1, a length scale over which momentum penetrates into the array and defined as the inner layer width [4], and δ_2, a length scale over which the shear extends into the main channel and defined as the outer layer width (see Fig. 1).

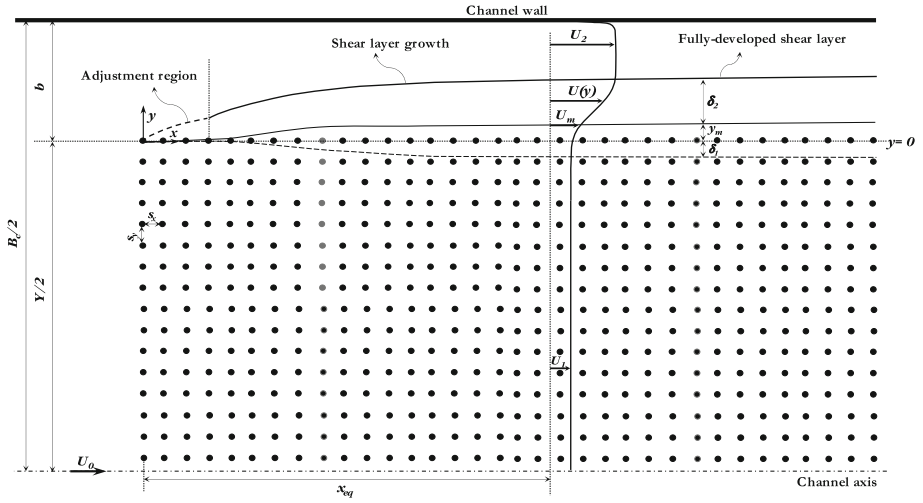

Fig. 1 Problem description at the interface between the obstructed and the unobstructed domains. Note: b is the width of the unobstructed area, x_{eq} is the equilibrium velocity length, defined as the distance from the leading edge of the array of cylinders to the downstream position at which the flow reaches a full-developed state ($\partial U/\partial x = 0$), U_0 is the mean channel velocity upstream of the cylinder arrays, and y_m (at which the velocity is indicated by U_m) is defined as the effective shear layer origin of δ_2, determined as the transversal position at which the local effect of the cylinders practically disappears and the flow velocity increases almost linearly

Despite the close resemblance between the flow distribution in the unobstructed flow area and that of a boundary layer feature on a flat-plate, White and Nepf [4] suggested that the unobstructed flow hydrodynamic structure is not identical to a developing laminar boundary layer. It is simply resembles a prototypical boundary layer form. The main difference between the laminar boundary layer on a flat-plate and the shear layer at the interface between the cylinder arrays and the unobstructed flow is related to the flow turbulence level. Due to the flow laminarity, the width of the boundary layer on a flat-plate is associated to the flow particle deceleration near the solid body caused by the viscous forces, which are the same order as the inertial forces. In the case of the laminar boundary layer, an insufficient momentum exchange takes place permitting the flow separation from the surface on a short downstream position x from the edge of the solid body. However, in the interface between the cylinder arrays and unobstructed flow, as reported in the present study, the velocities of the flow particles are not null but have considerable values and then the flow is full-turbulent [8].

Velocity distribution in uniform open-channel flows was widely discussed in several previous studies [23–26]. The open channel flow is composed of two regions [24, 25]; the inner-wall region where the flow is directly affected by the bed and the outer region where the flow is only indirectly affected by the bed through its shear stress, herein y is the point distance from the wall. The inner-wall region is further composed by three sub-region; the viscous sub layer, the buffer layer and the log-law layer. The inner-wall region is controlled and characterized by the friction velocity, u^*, and the fluid kinematic viscosity, v, that is the law of the wall. However, the outer region is characterized by the flow depth and the maximum mainstream velocity. Authors [24, 25] observed that the velocity in the outer region deviate upward from the log-law and is described empirically by the log-wake law (Fig. 2).

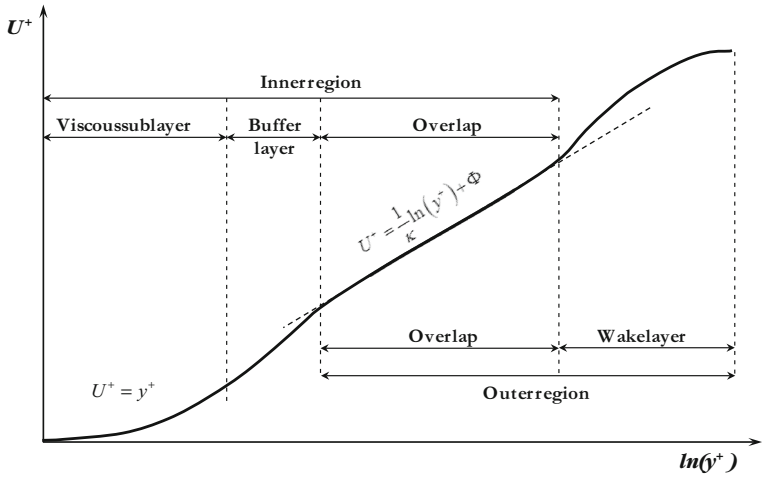

Fig. 2 Sketch of a classical representative velocity profile in open-channels

Velocity profiles are usually interpolated using laws belonging to one of two families: logarithmic laws and power laws. The best known velocity distribution law is still the logarithmic law of the wall [26]. The law of the wall governs the wall region in which the characteristic scales of length and velocity are $v/u*$ and $u*$, respectively. The logarithmic law of the wall is usually written as follows:

$$U^{+} = \frac{1}{\kappa}\ln(y^{+}) + \Phi\left(k_s^{+}\right) \tag{1}$$

where $U^{+} = U/u*$, $y^{+} = u*y/v$, $k_s^{+} = u*k_s/v$, U is the local time-averaged velocity, κ is the Von Karman's constant, k_s is representative of roughness height, v is the water kinematic viscosity and Φ is a function.

As mentioned above, the law of the wall governs a wall region, which means the presence of no-slip condition at the wall, and thus the flow velocity should be null at the solid boundary. In this study, the interface between the cylinder arrays and the unobstructed area is permeable, and then the no-slip condition is not available, whereas a slip flow condition occurs. At the interface, the flow velocity is not null, but it is of considerable magnitude and the flow is full turbulent. In order to adapt the law of the wall to the present study, it must rescale the flow conditions at the interface to resemble the application conditions of this law, i.e., zero velocity at the effective shear layer origin and characteristic scales of length and velocity similar to $v/u*$ and $u*$. Because the flow is full turbulent at the interface we adapted a length scale as v_t/u^{*}, where v_t is the eddy viscosity. Finally, Eq. (1) can be written as follows:

$$\frac{U - U_m}{u*} = \frac{1}{\kappa}\ln\left(\frac{(y - y_m)u*}{v_t}\right) + \Phi \tag{2}$$

The eddy viscosity is determined as:

$$v_t = \frac{u*^2}{\left(\frac{dU}{dy}\Big|_{y=y_m}\right)} \tag{3}$$

From Eq. (2) the velocity deficit at the interface region can be determined as:

$$U - U_m = \frac{u*}{\kappa}\ln(y - y_m) + \frac{u*}{\kappa}\ln\left(\frac{u*}{v_t}\right) + u * \Phi \tag{4}$$

It is also possible to write Eq. (4) as follows:

$$U - U_m = A\ln(y - y_m) + B \tag{5}$$

where

$$A = \frac{u*}{\kappa} \tag{6}$$

and

$$B = \frac{u*}{\kappa}\ln\left(\frac{u*}{v_t}\right) + u * \Phi \tag{7}$$

From Eq. (6), it can be noted that when the experimental velocity deficit ($U - U_m$) fits a single line as a function of $ln(y - y_m)$, the value of A can easily be determined. Consequently, the friction velocity $u*$ can also be obtained, taking into account the value of Von Karman's constant ($\kappa \approx 0.412$).

3 Experimental method

The experimental runs were carried out in a smooth horizontal rectangular channel at the Coastal Engineering Laboratory (L.I.C.) of the Department of Civil, Environmental, Building Engineering and Chemistry at the Technical University of Bari, Italy. The channel consisted of a base and lateral walls made of glass. The channel is 15 m long, 4 m large and 0.4 m deep. To create a current inside the channel, a closed hydraulic circuit was constructed. The water was pumped, from a large downstream metallic tank, by means a Flygt centrifugal electro-pump to the upstream steel tank. A side-channel spillway with adjustable height made from different plates mounted together was fitted into the upstream tank. The water that overflowed was discharged into the large metallic tank located downstream of the channel. Two different electromagnetic flow meters were mounted onto the hydraulic circuit of the channel, in order to measure both the pumped and the overflowed flow rates. The channel discharge Q was determined as the difference between the two flow rates. To create a smooth flow transition from the upstream tank to the flume, a set of stilling grids were installed in the upstream tank to dampen inlet turbulence. The upstream and downstream gates were used to define the flow depth and mean velocity in the channel (Fig. 3).

The model array was constructed of vertical, rigid, circular and threaded steel cylinders. The cylinder height, h, and diameter, d, were 0.31 m and 0.003 m, respectively. The cylinder extremities were inserted into a plywood plaque 3.0 m long, 4.0 m wide and 0.02 m thick, which in turn was fixed along the channel bottoms, forming the obstructed area of 3 × 3 m. It should be taken into account that the arrays of cylinders were partially mounted on the bottom of the channel, in the central part, leaving two lateral areas, each of them is 0.5 m large, of free flow circulation near the walls. The plywood plaque was extended 3 m both upstream and downstream of the array of cylinders (experimental area) and was tapered to the channel bottom to minimize flow disturbance. Cylinders were

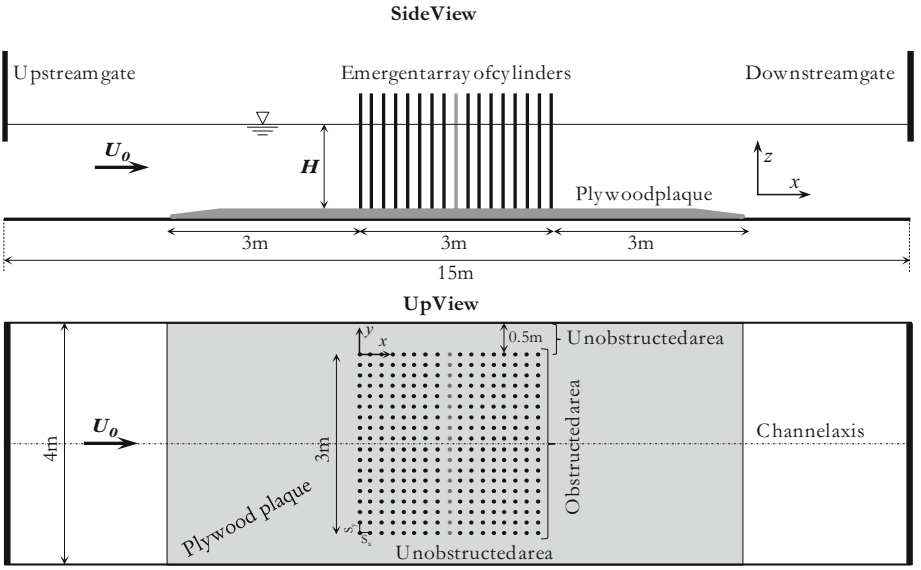

Fig. 3 General sketch of the laboratory flume with the experimental area

arranged regularly and spaced longitudinally, s_x, and transversally, s_y, with the same distance $s_x = s_y = 5.0$ cm, so that the cylinder density, n, was 400 cylinders/m^2.

The origin of the x-axis ($x = 0$) was taken at the leading edge of the array of cylinders, while the origin of the y-axis ($y = 0$) was taken at the array edge (Fig. 1). Because water is forced to move around the cylinders, the flow within the cylinder arrays is turbulent and highly heterogeneous at the scale of the individual cylinder. Therefore, the instantaneous three-dimensional flow velocity components, through different longitudinal, cross and horizontal planes, were accurately measured (1 cm × 1 cm grid resolution) using a three-dimensional (3D) Acoustic Doppler Velocimeter (ADV) system, together with CollectV software for data acquisition and ExploreV software for the data analysis, all produced by Nortek. The ADV was used with a velocity range equal to ±0.30 m/s, a velocity accuracy of ±1 %, a sampling rate of 25 Hz, a sampling volume of vertical extend of 9 mm and a time of acquisition window of order 2 min. A 15 db signal-to-noise ratio (SNR) and a correlation coefficients larger than 70 % are recommended by the manufacturer for high-resolution measurements. The acquired data were filtered based on the Tukey's method and the bad samples (SNR <15 db and correlation coefficient <70 %) were also removed. Because of the configuration of the ADV of downlooking probe probes, the uppermost 7 cm of the flow could not be sampled [3]. Additional details concerning the channel setup and the ADV operation can be found elsewhere in Ben Meftah et al. [26, 27] and Ben Meftah et al. [28].

The initial experimental conditions and parameters of the investigated runs are shown in Table 1. Herein, T is the water temperature, $Re_0 = U_0H/\nu$ is the inlet Reynolds number, $Fr_0 = U_0/(gH)^{0.5}$ is the inlet Froude number, $Re_2 = U_2H/\nu$ is the Reynolds number in the unobstructed area and $Fr_2 = U_2/(gH)^{0.5}$ is the Froude number in the unobstructed area, U_0 is the mean channel velocity and g is the gravity acceleration. The solid fraction of cylinders was constant for all the experimental runs having a value of $\varphi = 0.0028$.

Table 1 Initial experimental conditions and parameters of the investigated runs of fully-developed flow

Runs	H (m)	U_0 (m/s)	U_2 (m/s)	U_m (m/s)	T (°C)	Re_0 (−)	Fr_0 (−)	Re_2 (−)	Fr_2 (−)
R1	0.25	0.100	0.220	0.087	20	25000	0.064	55050	0.141
R2	0.22	0.114	0.247	0.101	09	17194	0.077	39331	0.168
R3	0.18	0.139	0.309	0.119	14	19555	0.105	47334	0.233
R4	0.14	0.179	0.385	0.162	15	20163	0.152	47193	0.329

4 Results and discussion

4.1 Shear layer development

Figure 4 shows an example of a vector map of the measured longitudinal velocity component U in both the obstructed and the unobstructed flow areas. The transversal profiles of U refer to run R3. The solid curve qualitatively represents the position of the nominal limit of the shear layer as a function of the ratio x/x_{eq}. x_{eq} is the equilibrium velocity length, see Fig. 1 for definition, determined experimentally, it is a longitudinal position from which $U(y)$ remains almost invariant as going further downstream (fully-developed flow). The numerous profiles of several measurement points for each one, as shown in Fig. 4, were taken in order to obtain as many details as possible on the flow development inside and outside the array of cylinders.

At the entrance section, where $x/x_{eq} \approx 0$, the U-profile appears of constant value along all the transversal direction y, except at the positions in line with the cylinders, where a reduction of U can be clearly noted, due to the known wake region formed downstream of each cylinder. When going further downstream from the entrance section, the magnitude of U starts to decrease gradually within the array of cylinders [19]. Outside the array the U-profiles, at $x/x_{eq} > 0.1$, are characterized by two typical regions: (i) a region immediately next to the interface between the array and the unobstructed flow domains, in which U increases continuously from a given velocity at the interface ($y = 0$) to a full velocity U_2, (ii) a free-stream region where U remains almost constant and equal to the full velocity U_2. It can be noted that, outside the array of cylinders, U almost behaves in the same way as a flow velocity close to a flat-plate [23]. Following and in the same way as the flow over a flat-plate, the first region will be defined as the shear layer, and behaves in exactly the same way as a rough boundary layer; the second region will be called the region of free-stream velocity. On the other hand, it can be seen that both the free-stream velocity U_2 and the velocity in the shear layer increase gradually with increasing distance from the leading

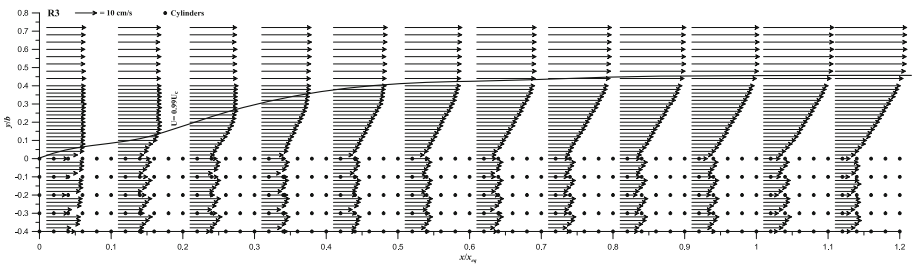

Fig. 4 Vector map of the U-velocity distribution for Run R3. The solid curve qualitatively represents the nominal limit of the shear layer, obtained at $U(y) = 0.99U_2$

edge of the array in the downstream direction. Starting from $x/x_{eq} \approx 0.70$, both U and U_2 velocities show a slight increase as x increases, tending to a state of almost fully-developed flow. According to the previous study by Rominger and Nepf [14], this can be explained by the transversal flow diversion, caused by the additional flow resistance due to the cylinder array drag. At the entrance of the obstructed area, Fig. 4 shows that the flow adjusts over a certain longitudinal distance x/x_{eq} of order 0.1, defined in Rominger and Nepf [14] as the interior length scale which is proportional to the cylinder array drag length scale and the cylinder array width ($Y/2$). The positive pressure gradient generated at the entrance of the obstructed area, due to the flow deceleration, causes transversal flow diversion. The absorption of this additional flow rate in the unobstructed area, keeping the flow depth H constant, is manifested by a slight velocity acceleration. It is worth noting that the proposed model refers to the region of fully-developed flow as the area where the shear layer width is almost constant ($\partial U/\partial x \approx 0$).

The shear layer width δ_2 was defined as the distance between the transversal position at y_m (see Fig. 1) and the position where the longitudinal component of the water velocity U is equal to 0.99 U_2. At any downstream position x outside the shear layer, it can be noted that U_2 remains of almost constant magnitude along the transversal direction. Despite the slight increase of U_2 as a function of x, upstream of the fully-developed flow region, δ_2 was determined defining at every position x the flow velocity U_2. Figure 4 shows that the shear layer width increases along the interface in the downstream direction. Near the leading edge of the array, at $x/x_{eq} \leq 0.11$, the thickness of the shear layer starts to increase with a slight rate, resembling in form the prototypical growth of the boundary layer in the initial laminar region of flat-plate turbulent boundary [23]. This is more pronounced in Fig. 5 for $x/x_{eq} \leq 0.15$. Figure 5 depicts the values of the normalized momentum thickness θ/θ_{eq} for all runs. The momentum thickness was calculated using the measured velocity profiles as:

$$\theta = \int_{y=y_m}^{\infty} \left(\frac{U - U_m}{U_2 - U_m}\right)\left[1 - \left(\frac{U - U_m}{U_2 - U_m}\right)\right] dy \tag{8}$$

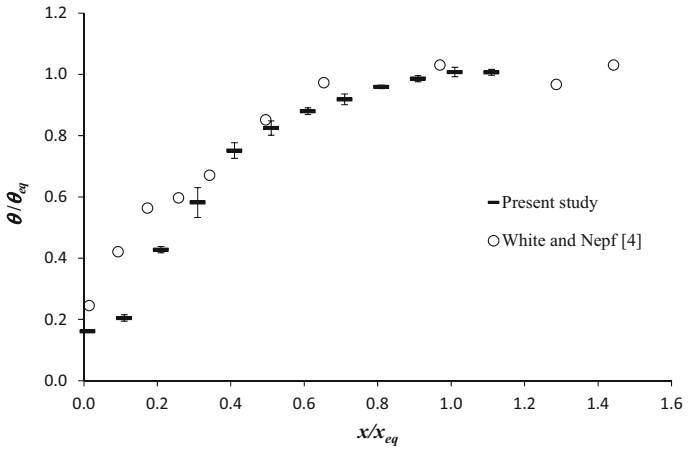

Fig. 5 Evolution of the momentum thickness. The values presented in this figure are the average of the calculated values of θ obtained with the different runs and the *vertical bars* are their standard deviations. The superposed data of White and Nepf [4] refer to run IV with $C_D a = 0.285$ cm^{-1}

The momentum thickness at the equilibrium stage is denoted by θ_{eq}.

Figures 4 and 5 show that, from $x/x_{eq} > 0.11$ to $x/x_{eq} \approx 0.5$, the shear layer width shows a clear sharp increase. Further downstream, $x/x_{eq} > 0.8$, the width of the turbulent shear layer tends to an almost constant value, where a fully-developed flow state is reached. As the shear layer width increases, the shear in the outer layer decreases indicating a net flux of momentum toward the shear layer. The momentum penetration is limited by the drag of the array of cylinders [4]. At the distance x_{eq} from the leading edge of the array of cylinders a maximum momentum penetration should be established leading to an equilibrium state of constant shear layer width.

Figure 5 clearly shows the growth of the momentum thickness with the increase of x, which is in agreement with the shear layer width evolution presented in Fig. 4. In addition to the momentum thickness data of the present study illustrated in Fig. 5, the superposition of the relative data digitalized from White and Nepf [4] has also been done. As clearly noted by Fig. 5, for $x/x_{eq} > 0.3$, the dimensionless momentum thickness for both cases shows a similar tendency; it behaves in the same manner and shows equal rates of growth. θ/θ_{eq} starts to increase slightly as x/x_{eq} increases and then asymptotes to an approximately constant value of order 1, suggesting the achievement of the fully-developed flow state. In contrast, for $x/x_{eq} \leq 0.3$, θ/θ_{eq} shows two different rates of growth. For the present study, θ/θ_{eq} increases slowly compared to White and Nepf's [4] study. This could be related to the additional flow resistance due to cylinder arrays drag. White and Nepf's [4] data refer to a cylinder arrays drag length scale, $(C_D a)^{-1}$, of order 4 cm against a value of order 60 cm for the present study. This means that for the cylinder arrays of highest solid volume fraction a strong upstream flow divergence occurred giving rise to low pressure at the leading-edge corner (more details in Rominger and Nepf [14]) which in turn leads to highest rate of the shear layer growth. As the solid volume fraction of the cylinder arrays becomes smaller this effect diminishes, giving rise to a smooth growth of the shear layer width, as shown in Fig. 5 for the present study.

For further confirmation of the equilibrium width of the shear layer, we plot, as an example, in Fig. 6 the transversal profiles of the normalized stream velocity $(U - U_m)/(U_2 - U_m)$ at different longitudinal positions x for run R2. Figure 6 shows that from $x/x_{eq} \geq 0.6$, all profiles are very close to one another. However, the profiles at $x/x_{eq} \geq 1$

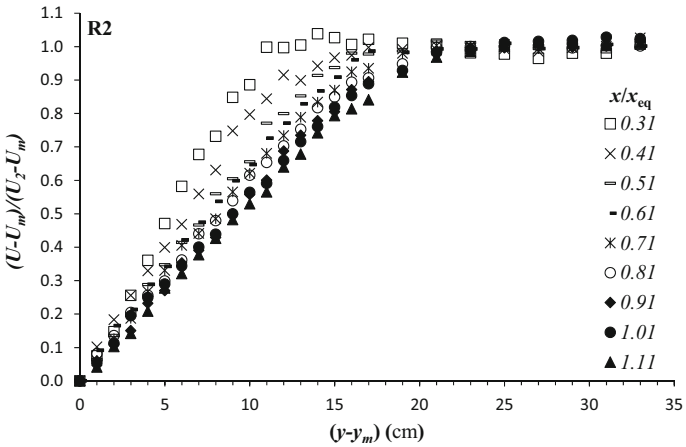

Fig. 6 Transversal profiles of the normalized stream velocity at different downstream positions x/x_{eq}

line up exactly, confirming the fully-developed flow occurrence where the width of the shear layer becomes almost invariant.

4.2 Adaptation of the law of the wall to the transversal velocity profile

The specific objectives addressed in this section are: (i) establishment of a new analytical model of the flow velocity distribution in the interface between the obstructed and the unobstructed flow areas based on the familiar universal law of the wall; (ii) introduction of specific flow velocity and transversal displacement parameters at the interface to adapt the law of the wall to the present study conditions; (iii) examination of the validity of the modified log-law model in producing the flow velocity distribution at the interface.

As clearly shown in Fig. 4, the flow velocity U almost behaves, as previously indicated, in the same way as a flow velocity close to a flat-plate, resembling a boundary layer feature. This supports the possibility of adapting the law of the wall to the transversal U-profiles in the interface region of the present study. Application of Eq. (2) requires before the determination of the friction velocity u^*, as a boundary condition. Usually, there are different ways of calculating u^* [29]: (i) from the log-law; (ii) from the measured Reynolds shear stress distribution; and (iii) using a global shear velocity based on the hydraulic radius. It is worth mentioning that in this study, due to the additional effect of transversal flow motion on δ_2, the friction velocity u^* should be determined using only the log-law procedure. In the current study, the value of u^* can be equal to the value of the square root of the maximum measured shear stress, if y_m coincides with the position of the shear stress peak, otherwise it experiences different values. If the peak of the measured shear stress takes place at a transversal position significantly greater than y_m, which is the case of this study, u^* shows a value greater than the square root of the maximum measured shear stress, recompensing the increase of δ_2 subjected to transversal flow motion, as observed by ben Meftah et al. [8].

In Fig. 7 we plot the flow velocity deficit $(U - U_m)$ versus $(y - y_m)$, in semi-logarithmic scale graph. The experimental data refer to runs R1 to R4. The plotted data

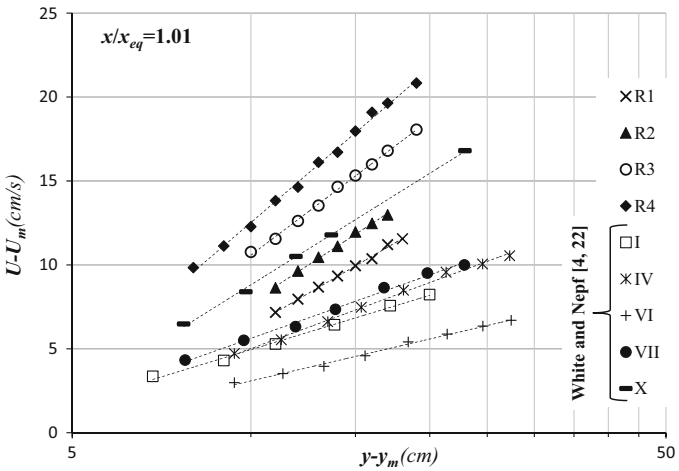

Fig. 7 Flow velocity deficit $(U - U_m)$ against $(y - y_m)$ in semi-logarithmic form, at the region of fully-developed flow

Table 2 Experimental values of the coefficients and physical properties presented in the different equations at the region of fully-developed flow

Runs	$C_D a$ (cm^{-1})	A	B	R^2	u^* (cm/s) predicted	u^* (cm/s) experimental	v_t (cm^2/s)	Φ	δ_2 (cm)
Present study									
R1	0.015	8.94	−14.28	0.99	3.69	1.22	20.58	0.30	22.5
R2	0.017	10.02	−15.32	0.99	4.13	1.34	21.32	0.28	21.0
R3	0.014	11.63	−16.19	1.00	4.79	1.30	21.45	0.26	20.8
R4	0.012	13.19	−17.84	1.00	5.43	1.50	24.01	0.32	21.5
White and Nepf [4, 22]									
I	0.092	4.67	−5.79	1.00	1.92	1.81	7.11	0.16	24.5
IV	0.285	5.67	−8.03	1.00	2.34	2.10	11.36	0.40	25.2
VI	0.255	3.60	−5.19	1.00	1.48	1.48	7.33	0.38	33.3
VII	2.430	5.45	−6.93	0.99	2.25	1.93	7.76	−0.07	29.2
X	1.770	9.58	−13.23	1.00	3.95	3.44	18.10	0.34	29.3
Average	–	–	–	–	–	–	–	0.26	–

R^2 is the square of the correlation coefficient relative to the linear regression (Fig. 7)

correspond to the longitudinal position $x/x_{eq} = 1.01$, where a fully-developed flow is reached. In addition to the experimental data of the present study, in Fig. 7 we also plot the data obtained by White and Nepf [4, 22] for five other different configurations, of various values of $C_D a$ (Table 2), with the aim to reflect the cylinder array density effect on the flow structure. In the current study, the White and Nepf's [4, 22] velocity data were digitalized from Fig. 16 of their paper [22]. As clearly shown in Fig. 7, $U - U_m$ fits a perfect single line as a function of $y - y_m$ for each run. The values of A and B, as shown by Eq. (5), are respectively determined, for each run, as the slope and the intercept of the regression line (dashed lines on Fig. 7). Based on Eq. (6) and taking into account a value of the Von Karman's constant κ equal to 0.412, the friction velocity u^* can be finally predicted (Table 2). In addition to the predicted values, the experimental values of u^*, calculated based on the maximum magnitude of the measured shear stress, were also illustrated in Table 2. Table 2 shows that the predicted values of u^* of the present study are considerably greater than those determined experimentally, this is due to the additional enlargement of δ_2 caused by the transversal flow motion generated by the cylinder arrays, as above indicated. While, for the previous studies of White and Nepf [4, 22], the predicted and experimental values of u^* are almost equal, due to the close coincidence of y_m and the position of the shear stress peak. Note that in White and Nepf's [4, 22] studies, the flow at the entrance of the array was separated from the unobstructed area of the channel flow by a 1.2 m long, splitter plate, allowing the flow to develop separately within each region, and minimizing transverse flow motions. In addition, it was observed, in a previous study [2], that the vegetation density affects the flow velocity at the interface. According to Naot et al. [2], with density values of the order of those used in White and Nepf [4, 22], see third paragraph in the introduction section, the flow in the obstructed area is gradually blocked, minimizing the transverse flow motions toward the unobstructed area. This may be explains why the peak in the equilibrium Reynolds stress profile appears close to the array edge (1–2 cm of it), which is quasi coincides with y_m.

The values of Φ were determined using Eq. (7) after defining the values of B. Note that, in the calculation of both the function Φ and the eddy viscosity v_t, obtained empirically using Eq. (3), we referred to the predicted friction velocity u^* (Table 2). For open-channel flows with smooth walls, Φ has a typical constant value of 5.3 regardless of the Reynolds and Froude numbers [24]. However, at the interface between the obstructed and the unobstructed flow areas, Φ shows (Table 2) small values compared to 5.3 for both the current study and those of White and Nepf [4, 22]. Table 2 shows that the predicted values of Φ varies slightly from run to run in a random order. It varies around an average value equal to 0.26 with a standard deviation of order 0.08 for all runs (of the present study and those of White and Nepf [4, 22]). This implies thatΦ can be considered almost constant ($\approx$0.3) regardless the Reynolds number, the Froude number and the cylinder array density $C_D a$. This finding strongly supports the idea of adapting the law of the wall to the transversal profile of the flow velocity at the interface. By the introduction of a determined v_t into the log-law, keeping the parameter κ equal to 0.412, it is worth mentioning that, in the current study, the integration constant Φ was empirically determined using the flow velocity measurements. In contrast, in other studies Φ is treated as a constant value and the characteristic roughness parameter (ν/u^*) as a variable to be determined. According to Stephan and Gutknecht [21], with the aim to define flow resistance due to the presence of submerged vegetation, the procedure used in many studies was the keeping of the integration constant Φ equal to 8.5 in addition to Von Karman's constant κ equal to 0.4 while varying the characteristic roughness parameter and the zero plane displacement.

Figure 8 depicts the profiles of the dimensionless velocity U^+ plotted versus the dimensionless transversal position y^+ in semi-logarithmic form for runs R1 to R4. On the same figure, we also plot some data obtained by White and Nepf [4, 22]. In Fig. 8, U^+ and y^+ are defined as: $U^+ = (U - U_m)/u^*$ and $y^+ = (y - y_m)u^*/\nu_t$. Both the classical theoretical curve of the log-law (solid line) for open-smooth-channel flows, of $\Phi = 5.3$ [30], and that of $U^+ = y^+$ (dashed line) are also plotted on Fig. 8. The dash-dotted line on Fig. 8

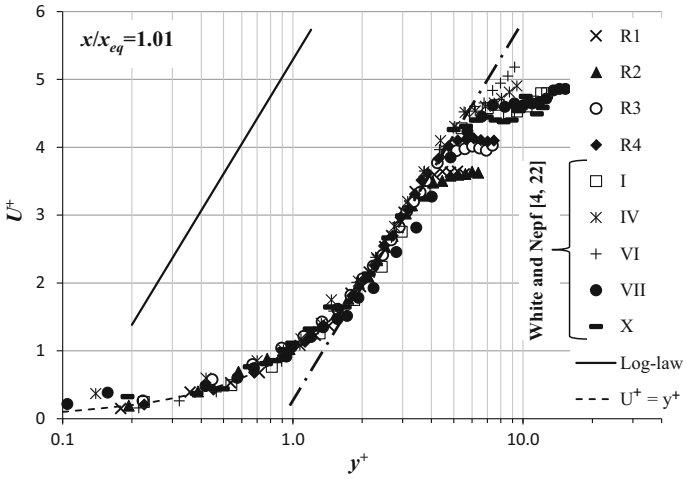

Fig. 8 Equilibrium transversal dimensionless velocity profiles U^+ versus y^+ in semi-logarithmic form

is simply the parallel of the log-law line, for open-smooth-channel flows, translated at the level of the illustrated data. Figure 8 shows that for $y^+ < 1.5$, all the data, for both the present and the previous studies, collapse onto a single fit and following the curve of $U^+ = y^+$. From $y^+ \geq 1.5$, all the data follow a single logarithmic trend. This logarithmic trend remains valid over a certain distance y^+, varies from run to run, and then the data experience a sharp deviation downward the log-law. The occurrence of the last deviation at different values of y^+ led to a shift of the profiles from each other, indicating an incomplete data similarity. The value difference between Φ determined in the present study and that of the typical log-law for open-smooth-channel flows (0.3 against 5.3, respectively), in addition to the incomplete similarity of all profiles shown in Fig. 8, points out the noticeable difference in the flow properties between both cases. At the interface between the obstructed and the unobstructed areas, the flow hydrodynamic structure is not identical to a developing laminar boundary layer, but simply the flow velocity distribution resembles a prototypical boundary layer form, as also confirmed by White and Nepf [4, 22].

The incomplete similarity of the data shown in Fig. 8 implies that the generated dimensionless velocity U^+ and length scales y^+ are not appropriate to represent all the data onto a single profile. In order to resolve this problem of data similarity, ulterior scaling of the flow velocity and the transversal coordinate, respecting always the log-law approach, should be done. Based on a previous study of Ben Meftah et al. [8], the rescale of the velocity and the length variables in the following way:

$$U^{++} = \frac{U - U_m}{U_2 - U_m} \text{ and } y^{++} = \frac{y - y_m}{\delta_2} \tag{9}$$

shows a good similarity between different profiles of U^{++} as a function of y^{++}. By comparing the data of the current study with those of previous studies reported in White and Nepf [4, 22], Ben Meftah et al. [8] confirmed that this similarity occurs independently of the flow and cylinder array characteristics, i.e. the Reynolds number, the Froude number and the cylinder array density. It is worth mentioning that in White and Nepf [4, 22] δ_2 was determined as $(U_2 - U_\mathrm{m})/\partial U/\partial y|_{ym}$, which differs from its definition used in this study. In the present study, the White and Nepf's [4, 22] δ_2, (Table 2) was determined in Ben Meftah et al. [8], using digitalized velocity data from White and Nepf [22], as the transversal distance between y_m and the position where U is equal to $0.99U_2$.

Taking into account the rescaled velocity U^{++} and transversal position y^{++}, as presented in Eq. (9), one can rewrite Eq. (2) as:

$$\frac{U - U_m}{\beta_1 u^*} = \frac{1}{\beta_1 \kappa} \ln\left[\beta_2 \left(\frac{(y - y_m)u^*}{\beta_2 \nu_t}\right)\right] + \frac{1}{\beta_1}\Phi \tag{10}$$

where β_1 and β_2 are respectively a dimensionless velocity and a dimensionless length parameters determined as follow:

$$\beta_1 = \frac{U_2 - U_m}{u^*} \text{ and } \beta_2 = \frac{\delta_2}{\left(\frac{\nu_t}{u^*}\right)} \tag{11}$$

Equation (11) can also be written as:

$$\frac{U - U_m}{\beta_1 u^*} = \frac{1}{\beta_1 \kappa} \ln\left(\frac{(y - y_m)u^*}{\beta_2 \nu_t}\right) + \frac{1}{\beta_1 \kappa} \ln(\beta_2) + \frac{1}{\beta_1}\Phi \tag{12}$$

and finally we can obtain an equation similar to Eq. (1) as:

$$U^+ + = \frac{1}{\beta_1 \kappa} \ln(y^{++}) + \Phi',$$

where

$$\begin{cases} U^{++} = \dfrac{U - U_m}{\beta_1 u^*} = \dfrac{U - U_m}{U_2 - U_m}, \\ y^{++} = \dfrac{(y - y_m) u^*}{\beta_2 \nu_t} = \dfrac{(y - y_m)}{\delta_2}, \\ \Phi' = \dfrac{1}{\beta_1 \kappa} \ln(\beta_2) + \dfrac{1}{\beta_1} \Phi. \end{cases} \tag{13}$$

The use of U^{++} and y^{++} instead of U^+ and y^+ is to mention the slight change that the formula has undergone compared to the classical log-law formula, as clearly manifested by the appearance of β_1 in the first term in the right hand side of Eq. (13).

Using the predicted friction velocity u^* (Table 2) and the measured physical properties U_2, U_m (Table 1) and δ_2 (Table 2), the values of β_1, β_2 and Φ' were easily determined, as shown in Table 3. The standard deviation of the parameters β_1, β_2 and Φ' (calculated based on the set of the nine runs presented in Table 3) are 0.48, 1.21 and 0.03 and their average are 4.27, 5.56 and 1.02, respectively. Compared to the average value the standard deviation of β_1, β_2 and Φ' can be almost considered of small value, which is more pronounced with β_1 and Φ'. This implies that β_1, β_2 and Φ' tend to be very close to their average values.

Figures 9a–c show the variation of three parameters β_1, β_2 and Φ' as a function of the cylinder array density $C_D a$, the Reynolds number Re_2 and the Froude number Fr_2, respectively, for the nine runs presented in Table 3. Figure 9 shows that the parameters β_1, β_2 and Φ' are almost invariant as a function of $C_D a$, Re_2 and Fr_2, especially Φ' and β_1. β_2 shows more scattering which mainly due to the difficulty to accurately estimate the eddy viscosity using the experimental data. Figure 9b indicates a slight decrease of β_1 and β_2 as a function of the Reynolds number which is less pronounced with β_1. Therefore and fore sake of simplicity, the values of β_1, β_2 and Φ' can be considered as constants in Eq. (13), regardless the cylinder array density, the Reynolds number and the Froude number. The non-dependence of β_1, β_2 and Φ' on the flow and cylinder array

Table 3 Calculated values of the parameters presented in Eq. (13)

Runs	β_1	β_2	Φ'
Present study			
R1	3.56	4.03	1.03
R2	3.54	4.07	1.04
R3	3.95	4.65	1.01
R4	4.06	4.87	1.03
White and Nepf [4, 22]			
I	4.64	6.63	1.02
IV	4.68	5.18	0.94
VI	4.83	6.74	1.04
VII	4.70	7.52	1.02
X	4.51	6.39	1.07
Average	4.27	5.56	1.02

characteristics leads to a general formula [Eq. (13)] capable of predicting the flow velocity distribution at the interface between the obstructed and the unobstructed areas in an open channel flow partially obstructed by an array of emergent cylinders/vegetation.

Figure 10 shows the transversal profiles of the experimental velocity, for both the present study and those of White and Nepf [4, 22], plotted as U^{++} versus y^{++} in a semi-logarithmic form. In contrast to Fig. 8, where only a partial similarity occurs between the experimental data, in Fig. 10 it can be clearly noted that all the data collapse onto a single profiles, confirming a complete similarity between them. In addition to the experimental data, in Fig. 10 we plot the predicted velocity profile using Eq. (13) with β_1 and Φ' of values equal to 4.3 and 1, respectively. As shown in Fig. 10, it can be observed that the logarithmic law presented by Eq. (13) is only applicable for $0.3 < y^{++} < 1$. In Fig. 10 we also plot the curve of $U^{++} = y^{++}$, making analogy with the viscous sub layer in open-smooth-channels (Fig. 2). In addition, the analytical power-law solution proposed by Ben Meftah et al. [8], as presented by Eq. (14), is also plotted in Fig. 10.

$$U^{++} = \frac{1}{2}\left[\left(\frac{\alpha_1}{L}\right)^2 + 4\frac{\alpha_2}{L}y^{++}\right]^{\frac{1}{2}} - \frac{\alpha_1}{2L} \quad \text{For } 0 \le y^{++} < 1$$

with

$$\alpha_1 = \frac{LU_m + V_m}{U_2 - U_m} \approx \frac{1.1LU_m}{U_2 - U_m}$$
$$\alpha_2 = \frac{gI\delta_2}{(U_2 - U_m)^2} \tag{14}$$

In Eq. (14) L is a secondary velocity intensity coefficient and $I = \partial H/\partial x$ is the energy slope, see Ben Meftah et al. [8] for more details.

For $y^{++} \le 0.3$, it can be clearly noted that the Ben Meftah et al.'s [8] analytical solution slightly overestimates the mean velocity U^{++}, however the solution of $U^{++} = y^{++}$ slightly underestimates it, and then the measured data are enveloped between them. Therefore, an average of both equations, as shown by Eq. (15), could be the suitable solution for the mean flow velocity distribution up to $y^{++} = 0.3$.

$$U^{++} = \frac{1}{4}\left[\left(\frac{\alpha_1}{L}\right)^2 + 4\frac{\alpha_2}{L}y^{++}\right]^{\frac{1}{2}} + \frac{1}{2}y^{++} - \frac{\alpha_1}{4L} \quad \text{For } 0 \le y^{++} < 0.3 \tag{15}$$

According to Ben Meftah et al. [8], in Eq. (15) the empirical constants L, α_1, and α_2 were experimentally estimated as 0.10, 0.07 and 0.17, respectively. The proposed solution of Eq. (15) is also plotted (dotted line) in Fig. 10. As you can see, the predicted velocity

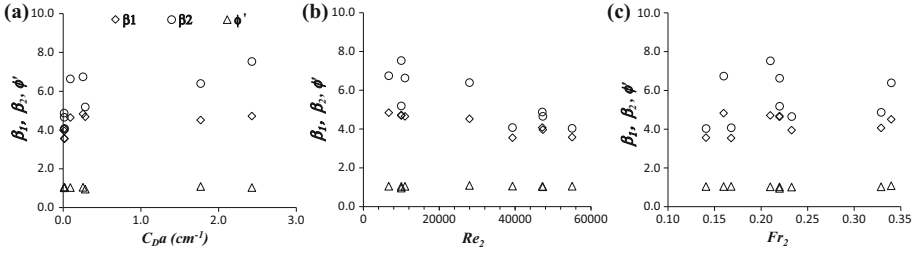

Fig. 9 Variation of β_1, β_2 and Φ' as a function of C_Da, Re_2 and Fr_2

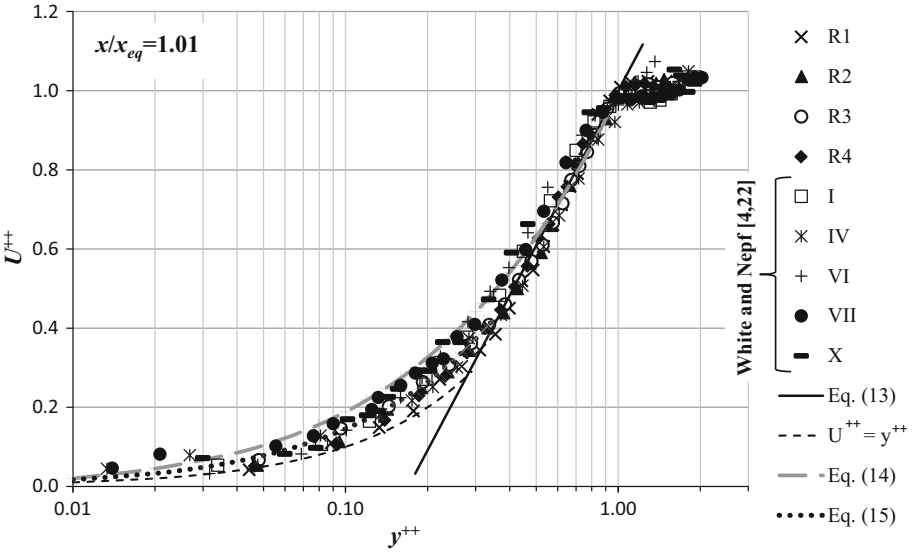

Fig. 10 The modified velocity profiles U^{++} versus y^{++} in semi-logarithmic form

profile determined by Eq. (15) seems to match well the experimental data trend for both the present and the previous studies. Figure 10 shows that, for $y^{++} \geq 1$, all the experimental data, for the different runs of the present and previous studies, collapse onto an almost single line of $U^{++} = 1$.

Summarizing the results of this section, it can be concluded that the analysis of flow velocity in partly obstructed channel flows led to the following results: (i) Seeing the resemblance in form between the shear layer, formed in partly obstructed channel flows, and the well-known boundary layer, formed in open-smooth-channel flows, an analytical modelling adapting the familiar logarithmic law to the flow velocity distribution at the interface between the obstructed and the unobstructed areas appears to be suitable and reasonable; (ii) introduction of the velocity deficit ($U - U_m$) is necessary to resemble the application conditions of the law of the wall, i.e., null velocity at the effective shear layer origin; (iii) the friction velocity u^*, as a boundary condition, is determined using the experimental data where the velocity deficit ($U - U_m$) fits a single line as a function of $ln(y - y_m)$, keeping a constant of Von Karman's κ equal to 0.412; (iv) because the flow is full turbulent at the interface between the obstructed and the unobstructed domains, an eddy viscosity v_t is adapted rather than the water kinematic viscosity v; (v) Adaptation of the classical logarithmic law to the transversal mean flow velocity distribution at the interface requires the introduction of specific rescaling of the velocity as U^{++} and the transversal coordinate as y^{++}; and (vi) a new modified log-law of the transversal profile of the flow velocity, at the interface between the obstructed and unobstructed areas in an open channel partially obstructed by an array of rigid and emergent cylinders/vegetation, is proposed as follows:

$$\begin{cases} U^{++} = \dfrac{1}{4}\left[\left(\dfrac{\alpha_1}{L}\right)^2 + 4\dfrac{\alpha_2}{L}y^{++}\right]^{\frac{1}{2}} + \dfrac{1}{2}y^{++} - \dfrac{\alpha_1}{4L} \quad \text{For} \quad 0 \le y^{++} < 0.3 \\ U^{++} = \dfrac{1}{\beta_1\kappa}\ln(y^{++}) + \Phi' \quad \text{For} \quad 0.3 \le y^{++} < 1 \\ U^{++} = 1 \quad \text{For} \quad y^{++} \ge 1 \\ \textit{with} \\ L = 0.1,\ \alpha_1 = 0.07,\ \alpha_2 = 0.17,\ \kappa = 0.412,\ \beta_1 = 4.3 \text{ and } \Phi' = 1 \end{cases} \tag{16}$$

By analogy with the classical representative velocity profile in open-channel flows, as shown above in Fig. 2, and based on the results obtained in this study, it can be concluded that the representative velocity profile at the interface between the obstructed and the unobstructed areas of partly obstructed channel flow is basically composed of two regions; the inner region ($y^{++} < 1$) and the outer region ($y^{++} \ge 0.3$) (Fig. 11). The inner region is further composed of the interface layer ($y^{++} < 0.3$) and the overlap (or the log-law) layer ($0.3 \le y^{++} < 1$). The outer region is also composed by two layer; the overlap layer and the free-stream layer ($y^{++} \ge 1$). The interface layer, as shown in Fig. 11, is virtually resembles in form the viscous sub layer, in open-channels, but is hydrodinamically different than it, due to the full turbulence flow at the interface. Comparable to open-channel flows [24, 25, 30], the interface layer is controlled by the inner variables such as the friction velocity u^* and the eddy viscosity v_t instead the water kinematic viscosity v. Since the variation from the inner region to the outer region is gradual, the overlap was also

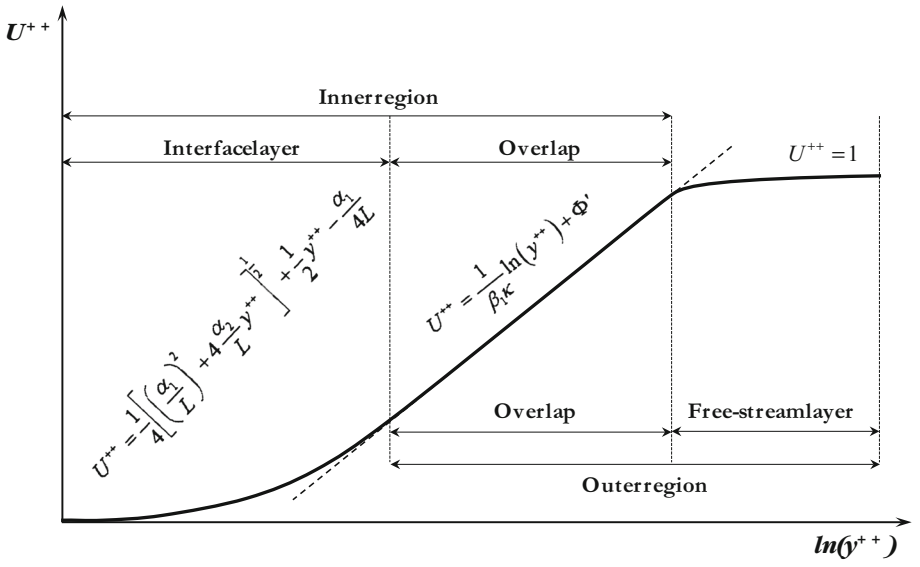

Fig. 11 Proposed sketch of the representative velocity profile at the interface between the obstructed and the unobstructed areas of partly obstructed channel flows

considered a part of the outer regions, it is an intermediate region where both effects of the inner and outer regions are combined. the outer region is controlled by the outer variables such as the flow depth H and the maximum mainstream velocity U_2. As shown in Figs. 10 and 11, at the free-stream region the velocity abruptly deviates downward the overlap region (log-law form) to a linear form of constant value, $U^{++} = 1$. It is to be noted that, the log-law, as shown in Eq. (16), is inherently valid (is continuous) both in the inner-interface region and in the free-stream region, and not only in the inner region as the cases of open-channels [30]. The deviation from the standard log-law region to the free-stream region does not require an additional function to adjust it, as is customary in boundary-layer and closed-channel analysis done by adding a wake function [24, 25, 30].

4.3 Analysis of turbulence intensities

To better understand the flow hydrodynamic structure at the interface between the obstructed and the unobstructed areas of partly obstructed channel flows, it is helpful to analyze the flow turbulence characteristics. The time of acquisition window was long enough to satisfy a constant local longitudinal mean velocity U and to establish a Gaussian frequency distribution of the velocity fluctuation u'. The tests carried out for the different runs showed that 3000 local velocity samplings (with an acquisition rate of 25 Hz) are widely sufficient to obtain a statistical stable estimation of U at any local position inside or outside the cylinder arrays (Fig. 12). Figure 12 shows the profiles of the ratio of the mean velocity U_N of N samplings ($10 \leq N \leq 3000$) against the mean velocity of the total samplings U_{3000} ($N = 3000$). Data refer to runs R1 to R4 and to different transversal position y: inside the array of cylinders [$(y - y_m)/(b - y_m) = -0.45$], at the interface between the obstructed and the unobstructed flow [$(y - y_m)/(b - y_m) = -0.04$], at almost the center of the shear layer [$(y - y_m)/(b - y_m) = 0.26$] and at the free-stream area [$(y - y_m)/(b - y_m) = 0.57$]. Figure 12 indicates that, at any position in the channel, the time of acquisition window was widely sufficient to put out a significant constant local mean velocity. Moreover, Fig. 13 shows that using the 3000 local velocity sampling, the values

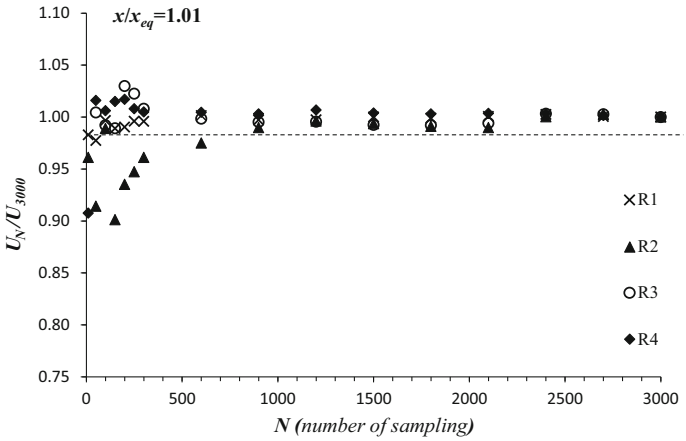

Fig. 12 Variation of the local mean velocity as a function of the sampling number, the illustrated sampling points were obtained at mid flow depth and at the normalized transversal position $(y - y_m)/(b - y_m) = 0.57$, 0.26, −0.04 and − 0.45 for R1, R2, R3 and R4, respectively

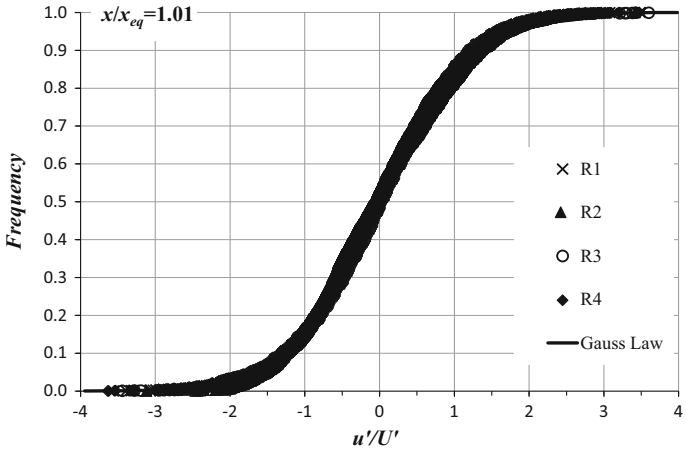

Fig. 13 Gaussian frequency distribution of the measured velocity fluctuation at $(y - y_m)/(b - y_m) = 0.57$, 0.26, −0.04 and −0.45 for R1, R2, R3 and R4, respectively

of the velocity fluctuation are distributed according to a Gauss law with mean zero. Herein, the u'-root mean square is defined as $U' = [(1/N)\Sigma(u'^2)]^{0.5}$.

In order to explore the distribution of energy in the signal across frequencies, example of the power spectral densities (PSD) of both the streamwise fluctuation $u'(t)$ and the spanwise fluctuation $v'(t)$ velocities are shown in Fig. 14. The data refer to run R2 and obtained at the transversal position of $(y - y_m)/(b - y_m) = 0.26$ (in the shear layer) and at the downstream position of $x/x_{eq} = 1$, where a fully-developed flow is established. In Fig. 14, we also plot the averaged PSD of the streamwise fluctuation, of run R2, obtained at the center of the obstructed area (obstructed area) $[(y - y_m)/(b - y_m) = -3.26, x/x_{eq} = 0.62]$, as reported in Ben Meftah and Mossa [19]. Note that, in the shear layer and for both velocity components, the spectrum of a frequency between 0.2 and 0.5 Hz, indicating the scaling subrange, is often referred to as the production subrange. This range

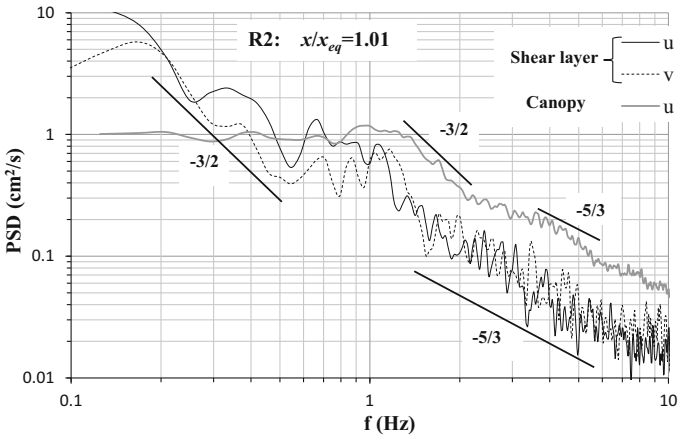

Fig. 14 Spectral distributions in the shear layer and within the array of cylinder

is characterized by a −3/2 spectral slope. Inside the obstructed area, however, the production subrange appears at a frequency between 1 and 2 Hz. At intermediate frequencies, 2–7 Hz, in the shear layer, an inertial subrange with a −5/3 spectral slope is observed. Inside the cylinder arrays, the spectral distribution obeys the −5/3 power law, however, in a narrow range of 4–7 Hz. This finding is in agreement with results obtained by Nezu and Onitsuka's [12] in a partly obstructed channel flow. Between the production subrange and the inertial subrange, a transitional subrange of frequency between 0.5 and 1, in the shear layer, and 2–4 Hz, inside the obstructed domain, is shown. In this subrange, a transformation of the turbulent energy of large scale motion (small frequency) to energy of small-scale motion (large frequency) takes place. For a frequency greater than 7 Hz, the PSD tends to very small values, indicating the start of the universal equilibrium range, where the energy input is in balance with the energy dissipation (no significant energy presence). This is more pronounced in the shear layer area.

Figure 14 clearly shows that, for a frequency greater than 1 Hz, the PSD has higher magnitudes within the array of cylinders compared to those obtained in the shear layer. This reveals a higher turbulent energy within the obstructed area due to the flow disturbance generated by the row of cylinders. White and Nepf [4] indicated that within the array of cylinders the velocity fluctuation are large compared with the local mean velocity U, while it is very small in the unobstructed flow area. This confirms the increase of PSD in the obstructed area compared to that obtained in the unobstructed one, as shown in Fig. 14.

Figure 15 shows the transversal profiles of the relative turbulence intensity U'/U of the longitudinal velocity component u for runs R1 to R4. The data refer to the downstream positions at $x/x_{eq} = 1.01$, zone of fully-developed flow. In Fig. 15 we also plot the data obtained by Laufer [31], Blinco and Partheniades [32] and White and Nepf [4, 22]. Note that the data of Laufer [31] and Blinco and Partheniades [32] refer to smooth open-channels with different Reynolds numbers Re, calculated based on the mean channel flow velocity U_0. The data of White and Nepf [4, 22] refer to a partly obstructed channel with different array densities, as previously mentioned (Sect. 4.2) and of Reynolds number Re_2 ranges between 1800 and 30,000.

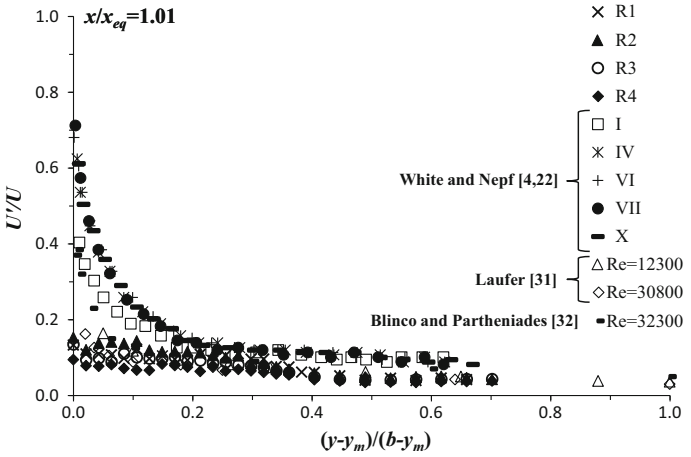

Fig. 15 Relative turbulence intensity profiles at the interface

Figure 15 indicates that the relative turbulence intensity profiles for the present and the previous studies show similar tendencies. U'/U starts to decrease gradually from $(y - y_m)/(b - y_m) = 0$, position of the effective shear layer origin, to attain the smallest values at the free-stream region. For $(y - y_m)/(b - y_m) < 2$, the data of White and Nepf [4, 22] show higher values of U'/U, ranging between 0.15 and 0.7. This can be explained by the small magnitude of the local velocity U of excessive fluctuation, at the interface. U'/U is greatly affected by the cylinder array density $C_D a$ (Table 2), as clearly shown in Fig. 13 in White and Nepf [4]. Within the array of cylinders and at the edge of the obstructed area, it can be clearly noted the increase of U'/U as $C_D a$ increases. This is also evidently observed in Fig. 15. The array density of the present study is almost six time smaller than the smallest density ($C_D a = 0.092$) reported in White and Nepf [4, 22], as shown in Table 2. This means that the values of U'/U of the present study should be smaller than those observed in White and Nepf [4, 22], which is clearly the case as shown in Fig. 15. Due to the small value of $C_D a$ in the present study, U'/U behaves in almost the same way as in smooth channel flows, as shown in Fig. 15 by the data of Laufer [31] and Blinco and Partheniades [32].

5 Conclusions

Despite significant previous studies [4, 8, 12, 22], it was observed that there still exists a lack of simple and efficient operative methods allowing the prediction of the main flow distribution at the interface between obstructed and unobstructed flow areas in a channel partially obstructed by array of rigid and emergent cylinders/vegetation. Numerous experimental studies conducted on submerged vegetated channels have shown that the vertical velocity profile above aquatic vegetation follows a logarithmic trend. Therefore, many of these studies adapted the universal logarithmic law, with specific modifications, to describe this velocity profile.

Analogous to what happened with submerged vegetated channels, at the interface between the obstructed and the unobstructed flow areas, of the present study and other previous studies, it was observed that the transversal profiles of the mean velocity almost behaves the same way as a vertical velocity profile above aquatic vegetation, resembling a boundary layer feature. This similarity between both cases, in addition to the similarity in feature of the flow velocity distribution at the interface to a boundary layer over a flat plate, made us adapting the universal logarithmic law of the wall to describe the transversal mean velocity profile at the interface in a partly vegetated channel, considering, by analogy, the interface as a virtual wall.

This study is limited to the region where the flow velocity profiles resembles a boundary layer. Note that the data within the obstructed region was discussed in a separate previous study by Ben Meftah and Mossa [19]. In contrast to the characteristics of the boundary layer on a flat plate, where the viscous shear stress plays an important role near the solid wall, at the interface between the obstructed and unobstructed areas the flow is full turbulent. This implies that, despite the resemblance in feature of the flow distribution between both cases, the hydrodynamic flow structure within the shear layer in partly obstructed channel is not identical as a boundary layer on a flat plate. This was taken into consideration in this study.

The specific objective addressed in this study is the proposal of a new modified log-law adapting the representative transversal profile of the flow velocity distribution, at the

interface between the obstructed and unobstructed areas in a channel partially obstructed by array of rigid and emergent cylinders/vegetation.

Summarizing the results of this study, it can be concluded that the analysis of flow velocity in partly obstructed channel flows led to the following results:

(1) because of the similarity in form between the shear layer, observed in partly obstructed channel flows, and the well-known boundary layer, formed in open-smooth-channel flows, an analytical modelling, adaptation the universal law of the wall, to predict the transversal profile of mean flow velocity at the interface between the obstructed and the unobstructed areas was suitable and reasonable;
(2) introduction of the velocity deficit $(U - U_m)$ is necessary to resemble the application conditions of the law of the wall, i.e., zero velocity at the effective shear layer origin;
(3) due to the additional enlargement of δ_2, caused by the transversal flow motion, the peak in the equilibrium Reynolds stress profile can be strongly shifted away from the array edge, depending on the array density. Therefore and in order to include almost all the transversal profile of flow velocity in our analysis, y_m is simply defined as the transversal position at which the local effect of the cylinders practically disappears and the flow velocity increases almost linearly. It is worth mentioning that, in some cases, y_m can coincide with the position of the shear stress peak;
(4) to recompense the increase of δ_2 subjected to transversal flow motion, the friction velocity u^*, as a boundary condition, is determined only using the experimental data where the velocity deficit $(U - U_m)$ fits a single line as a function of $ln(y - y_m)$, keeping a constant of Von Karman's κ equal to 0.412;
(5) because the flow is full turbulent at the interface between the obstructed and the unobstructed domains, we adapted an appropriate eddy viscosity ν_t instead of the water kinematic viscosity ν;
(6) adaptation of the classical logarithmic law to the transversal representative mean flow velocity profile, at the interface, requires the introduction of specific rescaling of the velocity as U^{++} and the transversal coordinate as y^{++};
(7) a new modified log-law of the transversal profile of the mean flow velocity, at the interface between the obstructed and the unobstructed areas in an open channel partially obstructed by an array of rigid and emergent cylinders/vegetation, is proposed and validated, as shown by Eq. (16),

As a part of second interest, detailed observations on the flow turbulence structure are also analyzed and discussed. The spectral analysis of the streamwise and spanwise velocities, inside and outside the array of cylinders, shows the formation of the three familiar production (−3/2 power law), transitional and inertial (−5/3 power law) sub-ranges, confirming the full-developed turbulent flow. It was also observed that the power spectral density has higher magnitudes within the array of cylinders as in the shear layer.

In the region of full-developed flow, the relative turbulence intensity profiles, for the present and previous studies, in both the partly obstructed channels and the smooth channels, follow similar tendencies. U'/U shows highest values at the effective shear layer origin, from which starts to decrease gradually to attain smallest values far from at the free-stream region. The relative turbulence intensity is greatly affected by the cylinder array density $C_D a$. It increases as $C_D a$ increases. Due to the small value of $C_D a$ in the current study, U'/U behaves in almost the same way as in smooth channel flows.

Acknowledgments The study was carried out at the Coastal Engineering Laboratory (L.I.C) of the Technical University of Bari, Italy, Department of Civil, Environmental, Building Engineering and Chemistry.

References

1. Thornton CI, Abt SR, Morris CE, Fischenich JC (2000) Calculating shear stress at channel-overbank interfaces in straight channels with vegetated floodplane. J Hydraul Eng 126(12):929–936. doi:10.1061/(ASCE)0733-9429
2. Naot D, Nezu I, Nakagawa H (1996) Hydrodynamic behavior of partly vegetated open channels. J Hydraul Eng 122(11): 625–633. ISSN 0733-9429/96/0011-0625-0633
3. Ghisalberti M, Nepf HM (2004) The limited growth of vegetated shear layers, Water Resour Res 40(7): W07502, 1–12. doi: 10.1029/2003WR002776
4. White BL, Nepf HM (2007) Shear instability and coherent structures in shallow flow adjacent to a porous layer. J Fluid Mech 593(12):1–32. doi:10.1017/S0022112007008415
5. Carollo FG, Ferro V, Termini D (2002) Flow velocity measurement in vegetated channels. J Hydraul Eng 128(7):664–673. doi:10.1061/(ASCE)0733-9429
6. Ghisalberti M, Nepf HM (2002) Mixing layers and coherent structures in vegetated aquatic flows. J Geophys Res 107(C2):1–11. doi:10.1029/2001JC000871
7. Shucksmith JD, Boxall JB, Guymer I (2011) Bulk flow resistance in vegetated channels: analysis of momentum balance approaches based on data obtained in aging live vegetation. J Hydraul Eng 137(12):1624–1635. doi:10.1061/(ASCE)HY.1943-7900.0000457
8. Ben Meftah M, De Serio F, Mossa M (2014) Hydrodynamic behavior in the outer shear layer of partly obstructed open channels. Phys Fluids 26(6): 065102, 1–19. doi: 10.1063/1.4881425
9. Hsieh PC, Shiu YS (2006) Analytical solutions for water flow passing over a vegetal area. Adv Water Resour 29(9):1257–1266. doi:10.1016/j.advwatres.2005.10.004
10. Pokrajac D, Manes C (2008) Interface between turbulent flows above and within rough porous walls. Acta Geophys 56(3):824–844. doi:10.2478/s11600-008-0022-1
11. Huai W, Geng C, Zeng Y, Yang Z (2011) Analytical solutions for transverse distributions of streamwise velocity in turbulent flow in rectangular channel with partial vegetation. Appl Math Mech-Engl Ed 32(4):459–468. doi:10.1007/s10483-011-1430-6
12. Nezu I, Onitsuka K (2001) Turbulent structures in partly vegetated open-channel flows with LDA and PIV measurements. J Hydraul Res 39(6):629–642. doi:10.1080/00221686.2001.9628292
13. Xiaohui S, Li CW (2002) Large eddy simulation of free surface turbulent flow in partly vegetated open channels. Int J Numer Meth Fluids 39:919–937. doi:10.1002/fld.352
14. Rominger JT, Nepf HM (2011) Flow adjustment and interior flow associated with a rectangular porous obstruction. J Fluid Mech 680(8):636–659. doi:10.1017/jfm.2011.199
15. Koch DL, Ladd AJC (1997) Moderate Reynolds number flows through periodic and random arrays of aligned cylinders. J Fluid Mech 349:31–66
16. Nepf HM (1999) Drag, turbulence, and diffusion in flow through emergent vegetation. Water Resour Res 35(2):479–489. doi:10.1029/1998WR900069
17. Lam K, Li JY, So RMC (2003) Force coefficients and Strouhal number of four cylinders in cross flow. J Fluids Struct 18(3–4):305–324. doi:10.1016/j.jfluidstructs.2003.07.008
18. Poggi D, Porporato A, Ridolfi L, Albertson JD, Katul GG (2004) The effect of vegetation density on canopy sub-layer turbulence. Boundary-Layer Meteorol 111:565–587
19. Ben Meftah M, Mossa M (2013) Prediction of channel flow characteristics through square arrays of emergent cylinders. Phys Fluids 25(4): 045102, 1–21. doi: 10.1063/1.4802047
20. Han Z, Zhou D, Gui X, Tu J (2013) Numerical study of flow past four square-arranged cylinders using spectral element method. Comput Fluids 84(9):100–112. doi:10.1016/j.compfluid.2013.05.008
21. Stephan U, Gutknecht D (2002) Hydraulic resistance of submerged flexible vegetation. J Hydrol 269(1–2):27–43. doi:10.1016/S0022-1694(02)00192-0
22. White BL, Nepf HM (2008) A vortex-based model of velocity and shear stress in a partially vegetated shallow channel. Water Resour Res 44(1): W01412, 1–15. doi: 10.1029/2006WR005651
23. Schlichting H (1955) Boundary layer theory. Pergamon Press, New York
24. Nezu I, Nakagawa H (1993) Turbulence in open-channel flows, IAHR monograph series. A. A. Balkema, Rotterdam. ISBN 9054101180
25. Nezu I, Asce M, Azuma R (2004) Turbulence characteristics and interaction between Particles and fluid in particle-laden open channel flows. J Hydraul Eng 130(10):988–1001. doi:10.1061/(ASCE)0733-9429(2004)130:10(988)

26. Ben Meftah M, De Serio F, Mossa M, Pollio A (2008) Experimental study of recirculating flows generated by lateral shock waves in very large channels. Environ Fluid Mech 8(6): 215–238. doi: 10.1007/s10652-008-9057-8
27. Ben Meftah M, De Serio F, Mossa M, Pollio A (2007) Analysis of the velocity field in a large rectangular channel with lateral shock wave. Environ Fluid Mech 7(6): 519–536. doi: 10.1007/s10652-007-9034-7
28. Ben Meftah M, Mossa M, Pollio A (2010) Considerations on shock wave/boundary layer interaction in undular hydraulic jumps in horizontal channels with a very high aspect ratio. Eur J Mech B/Fluids 29: 415–429. doi: 10.1016/j.euromechflu.2010.07.002
29. Babaeyan-koopaei K, Ervine DA, Carling PA, Cao Z (2002) Velocity and turbulence measurements for two overbank flow events in river Severn. J Hydraul Eng 128(10):891–900. doi:10.1061/(ASCE)0733-9429(2002)128:10(891)
30. Nezu I, Rodi W (1986) Open-channel flow measurement with a laser Doppler anemometer. J Hydraul Eng. ASCE 112(5):335–355. doi:10.1061/(ASCE)0733-9429(1986)112:5(335)
31. Laufer J (1951) Investigation of turbulent flow in a two-dimensional channel. NACA Report No. 1053: 1247–1266
32. Blinco PH, Partheniades E (1971) Turbulence characteristics in free surface flows over smooth and rough boundaries". J Hydraul Res 9(1):43–71